J Solid State Electrochem (2011) 15:1227–1233
DOI 10.1007/s10008-010-1189-3

ORIGINAL PAPER

Electrochemical behaviour of $YBaCo_4O_7$ in alkaline aqueous solution

Mircea Dan · Valerie Pralong · Nicolae Vaszilcsin · Andrea Kellenberger · Narcis Duteanu

Received: 21 June 2010 / Revised: 31 August 2010 / Accepted: 1 September 2010 / Published online: 18 September 2010

Abstract The paper presents the electrochemical investigation of mixed oxide $YBaCo_4O_7$ in alkaline aqueous solution during oxygen insertion/release. The electrochemical behaviour of $YBaCo_4O_7$ has been studied by cyclic voltammetry and electrochemical impedance spectroscopy. In correlation with these techniques, the compound morphology was determined by scanning electron microscopy. Based on the results obtained, the electrochemical processes occurring at the interface mixed oxide ($YBaCo_4O_7$)/electrolyte solution have been identified, and furthermore a mechanism of $YBaCo_4O_7$ oxidation/reduction in alkaline aqueous solutions has been proposed.

Keywords Mixed oxides · $YBaCo_4O_7$ · Electrochemical behaviour of $YBaCo_4O_7$ · Cyclic voltammetry · Electrochemical impedance spectroscopy

Introduction

During the last years, the 114 mixed cobalt oxides (with general chemical formula $ABCo_4O_7$, where A represents a trivalent metal and B represents a divalent metal) were one of the most investigated transitional metal mixed oxides due to their structural, magnetic and electric properties. There is a wide range of possible applications for these mixed cobalt oxides, as they were recommended as oxygen-permeable membranes, oxygen sensors and also fuel cell electrodes [1–5].

The $YBaCo_4O_7$ ceramic compound, also known as Y-114, was first reported by Valldor et al. in 2002 [6, 7], but the synthesis process and mixed oxide crystalline structure were explained in 2004 [7]. Regarding the electrochemical studies presented in this paper, it is relevant to mention that in each unit cell there are two different Co cations, Co^{2+} and Co^{3+}, with an atomic ratio of 3:1. The presence of these two cations in each unit cell gives a predominantly ionic character of this compound [3, 7, 8]. We also need to mention that the electrochemical behaviour of the Y-114 compound is determined by the mixed ionic and electronic conductivity [9] with a main contribution of p-type electronic conduction and a small contribution of the oxygen ionic conductivity estimated to be around 0.02% [10].

Until now, the oxidation capacity of Y-114 compound and also the reversibility of the oxidation process have been studied using only thermogravimetric measurements carried out under oxygen flow. Thus, oxidation capacities of the compound up to $YBaCo_4O_{7+\delta}$, where $\delta = 1.3 \div 1.54$, were obtained [1–3, 11, 12].

The present paper aims to elucidate the electrochemical behaviour of $YBaCo_4O_7$ mixed oxide at anodic and cathodic polarization in alkaline aqueous solution. Given the possibility of electrochemical intercalation of oxygen atoms in cobaltites [13–15], the alkaline medium was chosen. The electrochemical impedance spectroscopy results were interpreted in terms of a model describing the insertion of O^{2-} ions into the host electrode. The particularity of this model is the presence of a Gerischer element which has been previously proposed to describe the

M. Dan (✉) · N. Vaszilcsin · A. Kellenberger · N. Duteanu
Faculty of Industrial Chemistry and Environmental Engineering,
University "Politehnica" of Timisoara,
P-ta Victoriei 2,
300006 Timisoara, Romania
e-mail: mircea.dan@chim.upt.ro

V. Pralong
Laboratoire CRISMAT, ENSICAEN, CNRS, Université de Caen,
6 Bd Maréchal Juin,
14050 Caen, France

alternating current (AC) response of a chemical–electrochemical-type reaction [16].

Experimental

The $YBaCo_4O_7$ compound was obtained using solid-state reaction, by mixing the precursors Y_2O_3 (Aldrich 99.99%), $BaCO_3$ (Aldrich 99.999%) and $CoO_{4/3}$ (Normapur 99.9%) according to the stoichiometric cation ratio. After decarbonization at 1,000 °C the powder was pressed in bars (2×2×10 mm). The later were fired in air for 48 h at 1,200 °C and then removed rapidly from furnace and set to ambient temperature [9, 11, 12, 17]. The surface morphology of the $YBaCo_4O_7$ samples has been characterized by scanning electron microscopy (SEM) using a FEI QUANTA 200 microscope.

All electrochemical studies were carried out using an Autolab PGSTAT 302N equipped with electrochemical impedance spectroscopy (EIS) module. The electrochemical cell was equipped with two graphite counter electrodes positioned symmetrically against the working electrode ($YBaCo_4O_7$ bar, S=0.5 cm^2) and a Ag/AgCl electrode as reference. All potentials in this work are given versus the reference electrode. A 1 mol L^{-1} KOH solution has been used as electrolyte during all electrochemical studies.

EIS measurements were carried out using the FRA module of Autolab 302N, in the frequency range from 0.001 Hz to 100 kHz and AC voltage amplitude of 10 mV. For each spectrum, 60 points were collected, with a logarithmic distribution of 10 points per decade. The experimental electrochemical impedance data were fitted to the electrical equivalent circuit by complex nonlinear least squares (CNLS) Levenberg–Marquardt procedure using ZView, Scribner Associates Inc. software.

Results and discussion

Preliminary attempts have shown that it is possible to separate the peaks associated with the electrochemical processes occurring at the interface $YBaCo_4O_7$–KOH 1 mol L^{-1} only if the potential scan rate is around 5 mV s^{-1}. The cyclic voltammograms recorded for $YBaCo_4O_7$ electrode are depicted in Fig. 1. The main feature of the cyclic voltammogram recorded starting from open circuit potential (OCP) is the appearance on the forward scan of an oxidation peak (2) around −0.1 V assigned to Co(II) oxidation ($Co(II) \rightarrow Co(III) + e^-$). At higher potentials, the current increase (3) was associated with the oxygen evolution reaction.

On the backward scan of the cyclic voltammogram, a low-intensity limiting cathodic current is observed

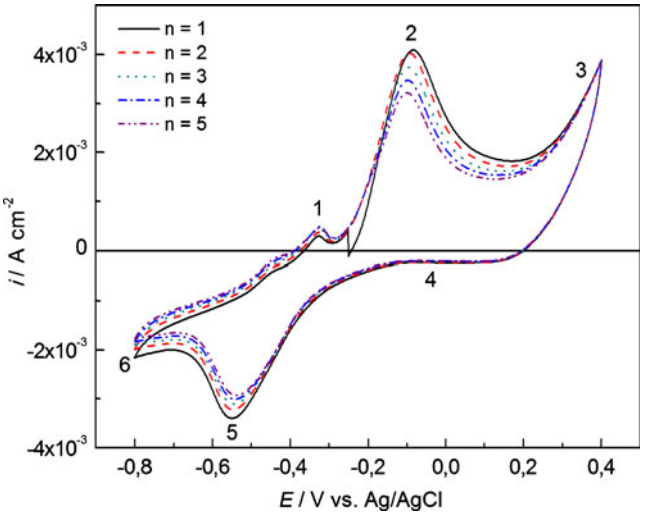

Fig. 1 Cyclic voltammograms (n=scan number) on $YBaCo_4O_7$ working electrode in 1 mol L^{-1} KOH solution at 5 mV s^{-1} scan rate

(marked on Fig. 1 with 4), and it was correlated with the reduction of remanent oxygen from the electrode surface, inside of crystal pores and also from the interstitial spaces between $YBaCo_4O_7$ crystallites. When the electrode potential shifts towards more negative values, a pronounced cathodic peak (5) associated with Co(III) reduction process ($Co(III) + e^- \rightarrow Co(II)$) appears around −0.55 V. At more negative electrode potentials, the current increase (6) is associated with the hydrogen evolution reaction.

Continuing the potential scan in the anodic direction up to OCP, a new oxidation peak (1) is observed at approximately −0.32 V due to superficial adsorbed hydrogen oxidation.

When the potential scan rate is increased, for example at 100 mV s^{-1}, the anodic part of the cyclic voltammograms changes. From Fig. 2, it can be noted that instead of the anodic peak (2) present in Fig. 1, a sigmoid wave was obtained, and the current density is almost double compared with the height of peak (2) from Fig. 1.

When the anodic potential sweep is performed at a higher scan rate, the amount of charge crossing the interface mixed oxide–electrolyte solution is not enough to oxidize all the Co(II) ions present at the interface, and in this way a limiting current appears, probably due to the slow diffusion of the electrolyte in the channels between crystallites. HO^- ions participate in electrode reaction in agreement with the mechanism proposed below. At a lower scan rate, the amount of charge crossing the interface is enough to oxidize almost completely the Co(II) ions from the interface, and consequently, the entire process becomes controlled by the oxygen diffusion inside the mixed oxide layer, and that leads to a pronounced peak.

An important factor influencing the oxidation process kinetics is the surface morphology which has been

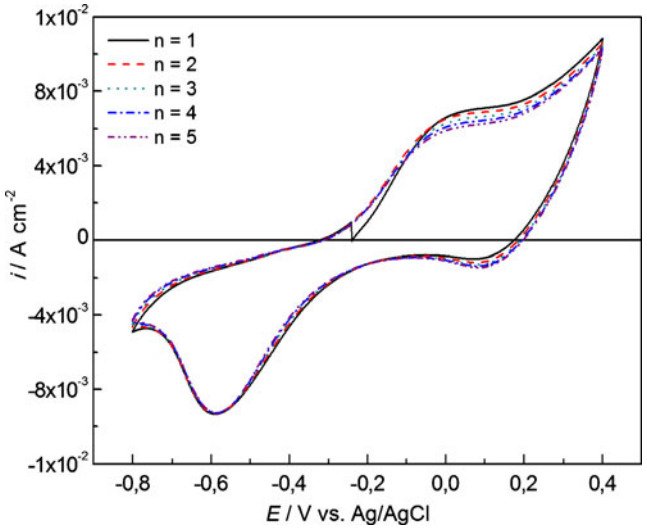

Fig. 2 Cyclic voltammograms (n=scan number) on $YBaCo_4O_7$ working electrode in 1 mol L^{-1} KOH solution at 100 mV s^{-1} scan rate

analysed using scanning electron microscopy. SEM images obtained for $YBaCo_4O_7$ bar electrode involved in this work are presented in Fig. 3. By analysing the SEM images, a porous structure due to crystallite agglomeration can be observed. Large pore amount leads to a higher specific surface with channels that favours oxygen adsorption/desorption process.

Based on all information presented above, a mechanism for the global oxidation process of $YBaCo_4O_7$ mixed oxide has been proposed (Fig. 4). In accordance with the proposed mechanism, at anodic polarization of $YBaCo_4O_7$ electrode, the oxygen ions' (O^{2-}) activity in the superficial layer becomes much higher than the oxygen activity in the bulk of mixed oxide. This activity gradient determines the oxygen diffusion inside $YBaCo_4O_7$ crystal simultaneously with the oxidation of Co(II) ions in the surface adjacent region. The rate of oxygen diffusion inside $YBaCo_4O_7$ crystallites is much slower than the rate of charge transfer reaction and the diffusion of hydroxyl ions from solution to the interface.

As a result, the electrochemical oxidation of $YBaCo_4O_7$ mixed oxide actually consists of the insertion of oxygen ions inside the $YBaCo_4O_7$ crystalline network. In consequence, during the oxidation process, the crystalline network becomes more compact and in this way further oxygen diffusion is restricted. Because of that, the oxidation of Co(II) to Co(III) is not complete, similar to the results obtained for chemical oxidation with molecular oxygen. This compaction of oxide layer leads to a slight irreversibility of the Co(II) oxidation process, as it can be seen from the decrease of oxidation (2) and reduction (5) peaks during consecutive potential cycling.

Diffusion of oxygen ions inside of crystallites leads to a superficial positive charge, which is compensated by hydroxyl ions arriving at interface by diffusion. When a water molecule is eliminated between adjacent hydroxyl ions, a new oxygen ion is formed at the interface which will diffuse in the bulk oxide. If the electrode potential is sufficiently positive, the oxygen evolution reaction occurs: $4\ HO^- \rightarrow O_2 + 4H^+ + 4e^-$.

According to the proposed mechanism, at anodic polarization after OCP, the Co(II) ion oxidation process is controlled by the charge transfer reaction. When the electrode potential becomes more positive, the entire process will be controlled by the diffusion of the electrolyte.

The impedance spectra recorded for the $YBaCo_4O_7$ electrode during oxidation at E=0.2 V are given in Fig. 5. The complex plane impedance plot can be divided into three zones corresponding to high, medium and low frequencies. At high frequencies, between 100 and 2.3

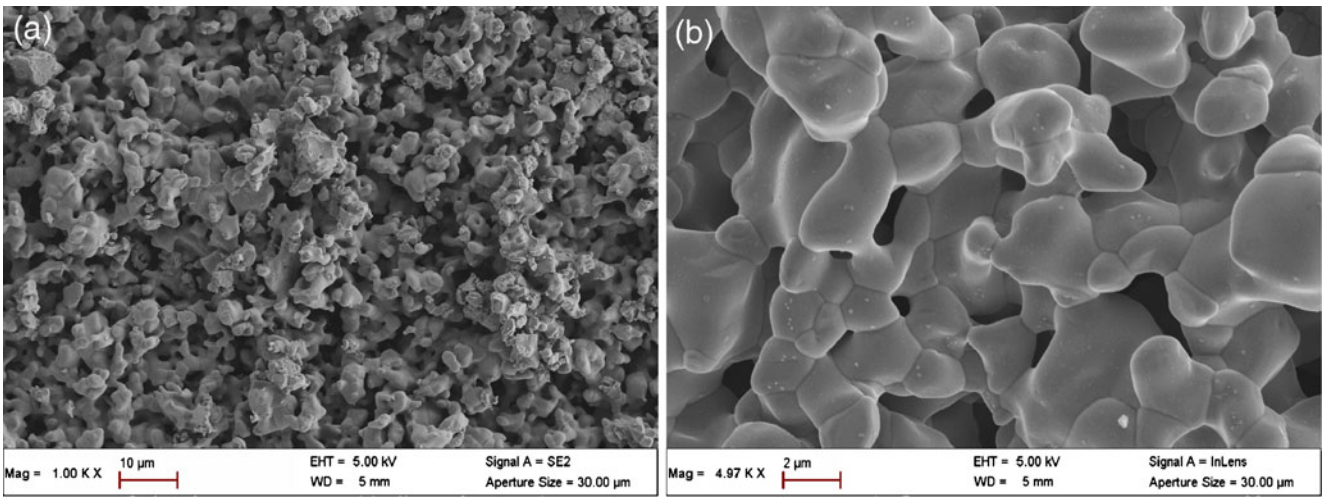

Fig. 3 SEM images of the $YBaCo_4O_7$ electrode's surface before electrochemical oxidation/reduction at ×1,000 (**a**) and ×5,000 (**b**) magnification

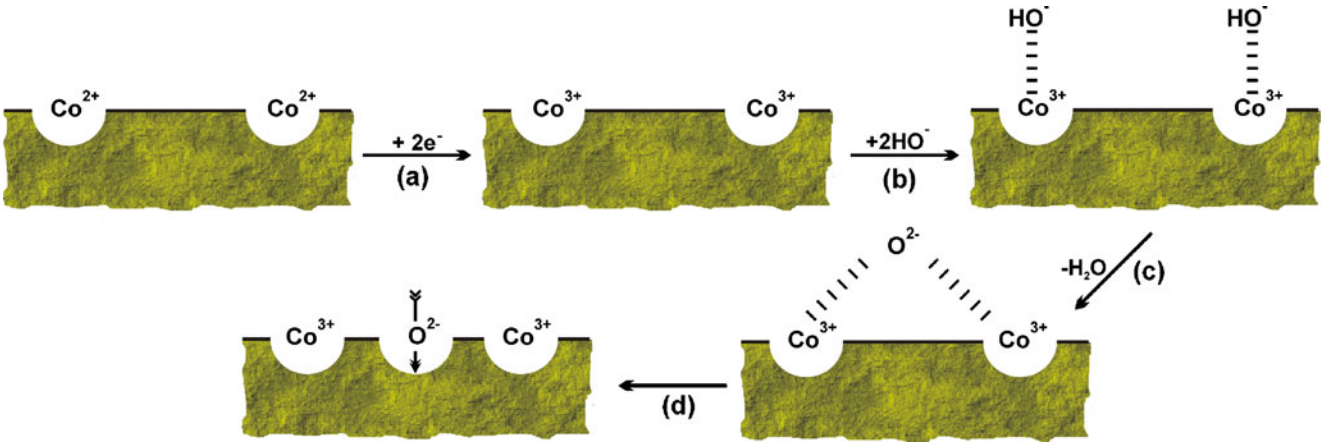

Fig. 4 Proposed mechanism for the electrochemical oxidation of $YBaCo_4O_7$ in alkaline solutions: *a* oxidation of Co^{2+} ions at electrode interface; *b* addition of HO^- ions at newly formed Co^{3+} cations; *c* elimination of water molecule and structural rearrangement of $YBaCo_4O_7$ compound; *d* diffusion of oxygen ions; *lines* preponderant ionic interaction

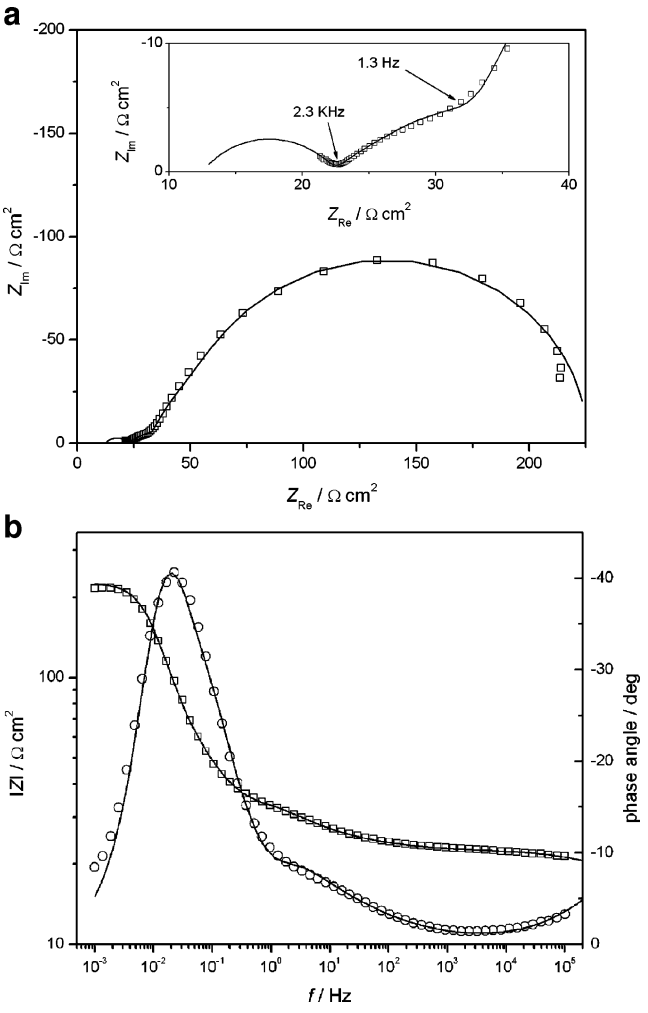

Fig. 5 Experimental Nyquist (**a**) and Bode (**b**) plots for $YBaCo_4O_7$ at E=0.2 V in 1 mol L^{-1} KOH. *Inset*: enlargement of the medium to high-frequency domain. *Open symbols* are experimental points and *continuous lines* are simulated by the CNLS fitting according to the equivalent circuit

kHz, the end of an incomplete semicircle can be observed, related to a charge transfer process. At intermediate frequencies, between 2.3 kHz and 1.3 Hz, a slightly curved line is obtained, related to a Gerischer element. Finally, at low frequencies, between 1.3 Hz and 1 mHz, another semicircle is observed.

The equivalent circuit used to model the experimental EIS data is given in Fig. 6, and it was derived from a similar model proposed for the insertion of Mg ions into the Mo_6S_8 Chevrel phase [18]. Unlike the model proposed by *Levi et al.*, in our model, the electronic and ionic conductions were not described by independent components in the equivalent circuit since it is known that for Y-114 the oxygen ionic conductivity has only a small contribution to the overall conductivity. The model proposed in Fig. 6 comprises a serial connection of the ohmic resistance (R_{Ohm}) and a parallel combination of the double-layer capacitance (CPE) and the charge transfer resistance (R_{ct}), followed by a Gerischer element (GE) and a parallel connection of a Warburg element (W) and a resistance (R) in series with a capacitor (C). The ohmic resistance represents a serial resistance including the uncompensated solution resistance and a contribution from the resistance of the $YBaCo_4O_7$ electrode. The double-layer capacitance is usually replaced by a constant phase element (CPE) to model small deviations from the ideal behaviour due to the surface roughness of the electrode. The impedance of a CPE is described by:

$$Z_{CPE} = 1/T(j\,\omega)^n \quad (1)$$

where T is a parameter related to the double-layer capacitance and n is an exponent between 0 and 1 describing the constant phase angle of the CPE.

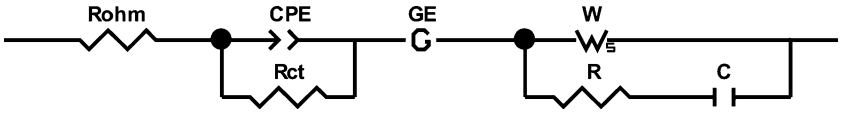

Fig. 6 Equivalent electric circuit for modelling oxygen insertion/release into the $YBaCo_4O_7$ electrode

The Gerischer element has been firstly used to model electrochemical systems where a chemical reaction is preceding or following the electrochemical reaction. The presence of a Gerischer element has been observed in case of mixed conducting solid electrolyte systems [19] and also during the insertion of Mg ions into the Mo_6S_8 Chevrel phases [18], and it is characteristic for systems involving a diffusion process coupled to a chemical reaction. In its most simple form, the impedance of a Gerischer element is given by:

$$Z_{GE} = Z_0/(k + \mathrm{j}\,\omega)^{1/2} \quad (2)$$

where Z_0 is the magnitude of the impedance at ω=1 rads^{-1} and k is a rate constant parameter.

The impedance of the Warburg element in case of a finite length thickness of the diffusion layer δ is given by:

$$Z_w = (R_w(\mathrm{j}\,\omega\tau_D)^{-\phi})\ \tanh\ (\mathrm{j}\,\omega\tau_D)^{\phi} \quad (3)$$

where R_w is the diffusion resistance, τ_D is the diffusion time constant given by $\tau_D=\delta^2/D$, with δ=diffusion thickness and D=diffusion coefficient and φ is an exponent between 0 and 1. This version of the Warburg element terminates in a finite resistance. At very low frequencies, the real part of the Warburg impedance approaches R_W, and the imaginary part goes to zero.

The experimental impedance data were fitted to the equivalent circuit using a CNLS procedure. The results of the fitting are shown as continuous lines in Fig. 5, and the corresponding values of the circuit elements together with their standard errors are given in Table 1. However, it should be noted that the determined kinetic parameters have apparent values since during the acquisition of the impedance spectra the conditions at the interface $YBaCo_4O_7$/electrolyte solution are not stationary.

Table 1 Experimental values of the circuit elements during oxidation of $YBaCo_4O_7$

Parameter	Value
R_{Ohm} [Ω cm^2]	12.5 (fixed)
T [F cm^{-2} s^n]	$7.28\times10^{-6}\pm0.71\times10^{-6}$
n	0.6 (fixed)
R_{ct} [Ω cm^2]	10.0±0.1
Z_0 [Ω cm^2 s$^{-1/2}$]	0.03976±0.00991
k [s^{-1}]	10.37±2.20
R_W [Ω cm^2]	194.5±1.6
τ_D [s]	35.82±1.26
Φ	0.5 (fixed)
R [Ω cm^2]	4.9±3.3
C [F cm^{-2}]	0.02512±0.00238

The high-frequency semicircle (HFS) was very well fitted only if the parameters solution resistance and phase angle of CPE were imposed because of the lack of experimental points in the high-frequency region. However, if the proposed model is used to simulate the response at high frequencies up to 10^8 Hz, the whole semicircle is visible as a continuous line in the inset of Fig. 5a. The constant phase angle parameter n has a value of 0.6 and is considered to be related to surface inhomogeneities and porosity of the electrode. Values around 0.9 are common for metal electrodes, while lower values of 0.6 have been reported for porous electrodes [20].

The charge transfer resistance and double-layer capacitance are related to the oxidation of superficial Co(II) ions to Co(III), corresponding to the first step denoted by (a) in the proposed electrochemical oxidation mechanism from Fig. 4. The higher value of the charge transfer resistance is common for solid-state reactions. Similarly, in case of the Warburg element, a high value of the diffusion resistance is indicative of the diffusion of oxygen ions inside the solid host electrode, more likely than for the diffusion of HO^- ions in the aqueous electrolyte solution.

The Gerischer impedance seems to be also related to a solid-state reaction, implying a chemical reaction, i.e. the formation of ionic bond between hydroxyl ions and superficial oxidized Co ions and/or the elimination of a water molecule between two adjacent hydroxyl ions corresponding to steps (b) and (c) in the proposed mechanism, followed by a slow diffusion of the oxygen ions through the mixed conductor/solution interface, step (d).

At cathodic polarization, like it was stated before, when the electrode potential is negative enough, the reduction of Co(III) ions will start. This will generate an excess of negative electric charges at the interface which will favour the migration of O^{2-} ions toward the electrolyte solution. Inside the interfacial double layer, the O^{2-} ions react with protons from neighbouring water molecules, forming HO^- ions. Since the beginning of reduction of Co(III) ions, the process is controlled by the diffusion of oxygen ions from the bulk toward the interface. The mechanism proposed for the reduction process is presented in Fig. 7.

The electrochemical impedance spectra for the reduction of $YBaCo_4O_{7+\delta}$ at E=−0.7 V shown in Fig. 8 give evidence to support the proposed mechanism. The complex

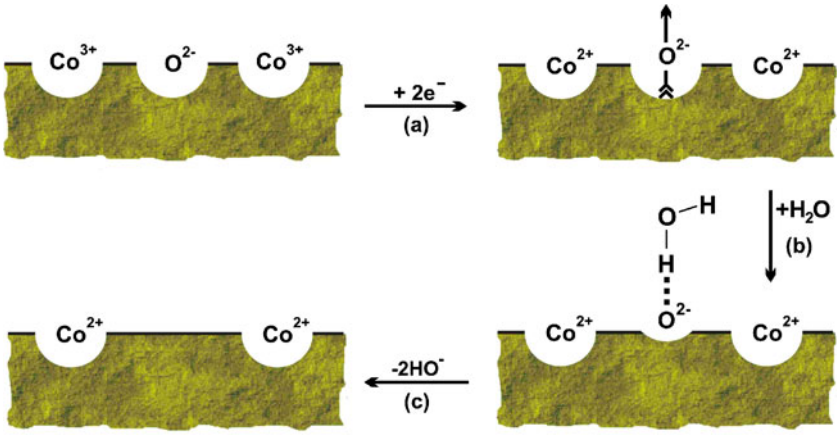

Fig. 7 Proposed mechanism for the electrochemical reduction of $YBaCo_4O_{7+\delta}$ in alkaline solutions: *a* reduction of Co^{3+} ions at electrode interface; *b* interaction of oxygen ion O^{2-} with water molecule; *c* extraction of H^+ from water molecule

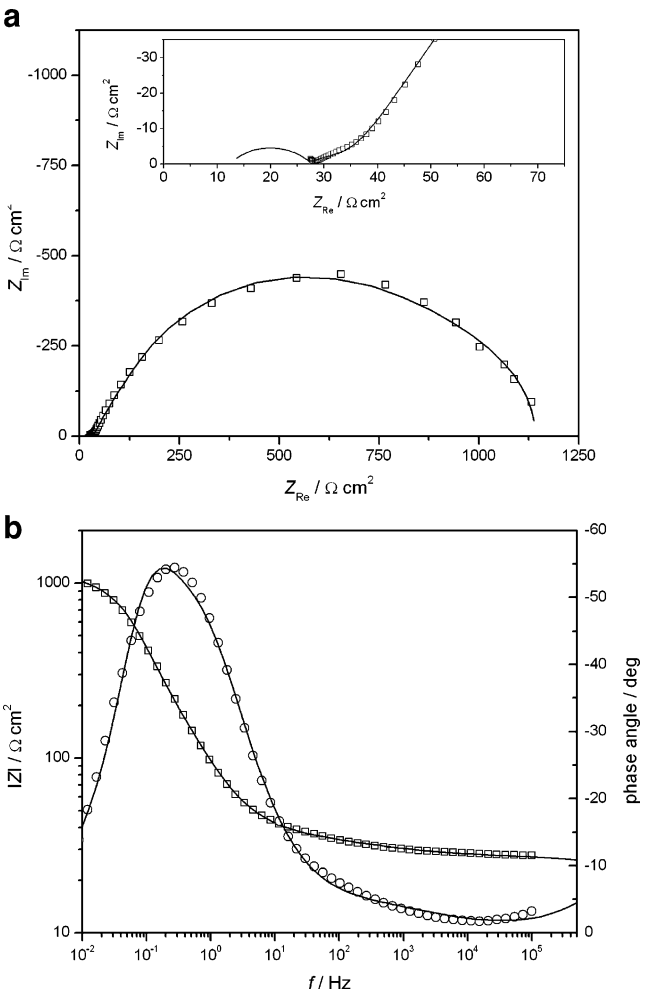

Fig. 8 Experimental Nyquist (**a**) and Bode (**b**) plots for $YBaCo_4O_{7+\delta}$ at $E=-0.7$ V in 1 mol L^{-1} KOH. *Inset*: enlargement of the medium- to high-frequency domain. *Open symbols* are experimental points and *continuous lines* are simulated by the CNLS fitting according to the equivalent circuit

plane plots present a similar shape to those obtained during the oxidation, consisting of an incomplete semicircle at high frequencies, followed by a slightly curved line at intermediate frequencies and a low-frequency semicircle. The EIS spectra obtained during reduction were modelled based on the same equivalent circuit as in the case of oxidation, and the corresponding results are given in Table 2. The HFS is related to a charge transfer process, the reduction of the superficial Co(III) ions to Co (II)ions. The negative charges generated at the electrode surface will promote the migration of O^{2-} ions from the bulk of the mixed conductor towards the electrolyte solution, reflected in the presence of Warburg diffusion impedance in the low-frequency region of the EIS spectra. The Gerischer impedance at medium frequencies is related to a chemical reaction coupled to the charge transfer reaction, i.e. the interfacial reaction between O^{2-} ions and water molecules.

Table 2 Experimental values of the circuit elements during reduction of $YBaCo_4O_{7+\delta}$

Parameter	Value
R_{Ohm} [Ω cm^2]	12.5 (fixed)
T [F cm^{-2} s^n]	$3.31\times10^{-7}\pm1.09\times10^{-7}$
n	0.7 (fixed)
R_{ct} [Ω cm^2]	14.7±0.1
Z_0 [Ω cm^2 $s^{-1/2}$]	0.0110±0.0005
k [s^{-1}]	0.045±0.003
R_W [Ω cm^2]	694.3±14.4
τ_D [s]	4.58±0.28
Φ	0.5 (fixed)
R [Ω cm^2]	6.2±0.5
C [F cm^{-2}]	$2.43\times10^{-3}\pm0.14\times10^{-3}$

Conclusions

Results obtained by cyclic voltammetry showed that the $YBaCo_4O_7$ mixed oxide is sensitive at anodic or cathodic polarization. Oxidation process consists in oxygen insertion in oxide structure. This insertion is initially controlled by charge transfer stage and also by the electrolyte diffusion in the channels between crystallites. After oxidation of superficial Co(II) ions, the entire process is slowed down because the rate-determining step becomes the diffusion of oxygen ions inside of oxide bulk. Oxygen diffusion leads to a compact crystallite structure, obstructing the complete oxidation of Co(II) ions. On the other hand, the reverse process (reduction) is controlled from the beginning by the oxygen ion diffusion from inside of the crystal to the interface. This mechanism leads to sharp reduction peaks on the cyclic voltammograms, unaffected by the scan rate. EIS spectra recorded during reduction at −0.7 V show that the rate-determining step is the charge transfer reaction of O^{2-} ions.

The compaction of Y-114 during oxidation imposes a partial irreversible character of the oxidation process, and as a consequence, the oxidation and reduction peak maxima decrease in time. Thus, a complete structural characterization of the fully oxidized phase will be discussed in a forthcoming paper.

Acknowledgement V. Pralong and M. Dan gratefully acknowledge the CNRS and the Minister of Education and Research for financial support through their Research, Strategic and Scholarship programmes (ANR-09-JCJC-0017 “TUNE”) and the European Union for support through the network of excellence Novelox.

References

1. Tsipis EV, Khalyavin DD, Shiryaev SV, Redkina KS, Núñez P (2005) Mater Chem Phys 92:33–38
2. Hao H, Cui J, Chen C, Pan L, Hu J, Hu X (2006) Solid State Ionics 177:631–637
3. Haoshan H, Limin Z, Jie H, Xing H, Hongwei H (2009) J Rare Earths 27:815–818
4. Tsipis EV, Kharton VV, Frade JR, Núñez P (2005) J Solid State Electrochem 9:547–557
5. Zhang K, Zhu Z, Ran R, Shao Z, Jin W, Liu S (2010) J Alloys Compd 492:552–558
6. Valldor M, Andersson M (2002) Solid State Sci 4:923–931
7. Valldor M (2004) Solid State Sci 6:251–266
8. Maignan A, Hébert S, Caignaert V, Pralong V, Pelloquin D (2008) Solid State Commun 147:470–473
9. Tsipis EV, Kharton VV, Frade JR (2006) Solid State Ionics 177:1823–1826
10. Kharton VV, Yaremchenko AA, Naumovich EN (1999) J Solid State Electrochem 3:303–326
11. Motohashi T, Kadota S, Fjellvag H, Karppinen M, Yamauchi H (2008) Mater Sci Eng B 148:196–198
12. Hao H, Chen C, Pan L, Gao J, Hu X (2007) Physica B 387:98–102
13. Grenier J-C, Wattiaux A, Doumerc J-P, Dordor P, Fournes L, Chaminade J-P, Pouchard M (1992) J Solid State Chem 96:20–30
14. Grenier J-C, Bassat J-M, Doumerc J-P, Etourneau J, Fang Z, Fournes L, Petit S, Pouchard M, Wattiaux A (1999) J Mater Chem 9:25–33
15. Pralong V, Caignaert V, Hebert S, Maignan A, Raveau B (2006) Solid State Ionics 177:1879–1881
16. Gerischer H (1951) Z Phys Chem 198:216
17. Caignaert V, Maignan A, Pralong V, Hébert S, Pelloquin D (2006) Solid State Sci 8:1160–1163
18. Levi MD, Gizbar H, Lancry E, Gofer Y, Levi E, Aurbach D (2004) J Electroanal Chem 569:211–223
19. Boukamp BA, Bouwmeester HJM (2003) Solid State Ionics 157:29–33
20. Kellenberger A, Vaszilcsin N, Brandl W (2007) J Solid State Electrochem 11:84–89